Society of Medical Education & Research

2022, Volume 2, Issue 1, Page No: 99-116
ISSN: 3108-4826

Journal of Medical Sciences and Interdisciplinary Research

Targeting Gefitinib-Resistant EGFR Mutants with Narciclasine in Non–Small Cell Lung Cancer

Yuki Haruto Tanaka[1]*, Kenta Naoki Sato[1]

[1]Department of Management, Hitotsubashi University Business School, Tokyo, Japan.

***E-mail** ✉ y.tanaka.hub@gmail.com

Abstract

Non-small cell lung cancer (NSCLC) involves aberrant epidermal growth factor receptor (EGFR) activation resulting from overexpression or mutations. Although EGFR tyrosine kinase inhibitors (TKIs) like gefitinib are employed in NSCLC therapy, resistance frequently emerges through secondary EGFR mutations or bypass signaling pathways. Thus, new agents capable of bypassing EGFR-TKI resistance are essential for improved NSCLC management. Narciclasine (Ncs) is a cytotoxic alkaloid derived from Narcissus species that demonstrates antitumor and anti-inflammatory properties.Cell viability was determined via trypan blue staining and Live/Dead assay. The antiproliferative activity of Ncs was examined using the WST-1 assay and cell cycle profiling in several NSCLC lines, including A549 and H1299 (wild-type EGFR), gefitinib-resistant H1975 (L858R/T790M-EGFR), gefitinib-sensitive PC-9 (exon 19 deletion-EGFR), and the gefitinib-resistant PC-9 derivative, PC-9-GR. Molecular docking simulations explored Ncs interaction with wild-type and mutant EGFR forms. The impact of Ncs on EGFR kinase function was tested in vitro using wild-type EGFR and L858R/T790M-EGFR. In vivo antitumor activity of Ncs was evaluated in a C. elegans model expressing L858R/T790M-EGFR and in mouse xenografts of A549 and H1975 cells. Tumor tissues underwent histological examination for EGFR, phosphorylated EGFR, and phosphorylated STAT3 expression.Ncs displayed potent growth suppression across diverse NSCLC lines, encompassing gefitinib-sensitive A549, H1299, and PC-9 cells as well as gefitinib-resistant H1975 and PC-9-GR cells. Remarkably, Ncs achieved an IC50 of 22 nM in H1975 cells harboring the gefitinib-resistant EGFR mutant, substantially lower than in other lines. Ncs strongly provoked G2/M phase arrest in H1975 cells. Docking studies indicated Ncs binding to both wild-type and mutant EGFR, with preferential inhibition of L858R/T790M-EGFR kinase activity over wild-type EGFR. In the C. elegans model, Ncs attenuated the tumor-like multivulva phenotype. Ncs administration reduced tumor progression in mice bearing A549 or H1975 xenografts and decreased EGFR, p-EGFR, and p-STAT3 levels in tumor samples. These findings indicate that Ncs exerts anticancer effects through suppression of EGFR function and associated downstream pathways. This action is especially pronounced in EGFR mutants conferring TKI resistance, including to gefitinib, highlighting Ncs as a promising candidate for treating TKI-resistant NSCLC.

Keywords: Narciclasine, NSCLC, EGFR-TKI resistance, Tumor samples

Introduction

Lung cancer remains the leading cause of cancer-related death in both men and women [1]. Key driver genes in lung cancer include EGFR, KRAS, MET, LKB1, BRAF, PIK3CA, ALK, RET, and ROS1 [2]. EGFR, a tyrosine kinase receptor, shows hyperactivity from overexpression or mutations in various malignancies, notably lung and breast cancers [3]. EGFR alterations are major oncogenic drivers in non-small cell lung cancer (NSCLC) [4]. Approximately 85% of detected EGFR kinase domain mutations consist of the L858R point mutation in exon 21 or in-frame deletions in exon 19 [5]. Both the L858R substitution and exon 19 deletions lead to ligand-independent constitutive EGFR activation and

Access this article online https://smerpub.com/

Received: 09 January 2022; **Accepted:** 11 March 2022

How to cite this article: Tanaka YH, Sato KN. Targeting Gefitinib-Resistant EGFR Mutants with Narciclasine in Non–Small Cell Lung Cancer. J Med Sci Interdiscip Res. 2022;2(1):99-116. https://doi.org/10.51847/iOdIctHVaP

prolonged phosphorylation [6]. Such mutants stimulate prosurvival and proliferative pathways, including AKT and STAT signaling [7]. To counter mutation-driven EGFR hyperactivity in NSCLC, ATP-competitive small-molecule inhibitors targeting the EGFR kinase domain were developed [8]. These tyrosine kinase inhibitors (TKIs) effectively block constitutively active EGFR by mimicking ATP [9]. In treatment-naïve advanced NSCLC patients with EGFR mutations, TKIs yield superior progression-free survival relative to conventional chemotherapy. First-generation agents erlotinib and gefitinib outperformed chemotherapy in this regard [10, 11]. Nevertheless, acquired resistance typically develops within 10–14 months despite initial responses. Multiple resistance mechanisms to erlotinib and gefitinib have been characterized, and elucidating them is vital for overcoming acquired resistance. The predominant mechanism involves the secondary T790M mutation in exon 20 [12]. This T790M change not only induces resistance to first-generation TKIs but also enhances EGFR kinase activity and downstream signaling, promoting tumor growth [13]. The third-generation TKI osimertinib was specifically engineered to target T790M-containing EGFR while sparing wild-type EGFR [14]. Although osimertinib shows strong efficacy against L858R/T790M NSCLC, new resistance patterns have appeared [15]. Consequently, additional therapeutic approaches are required for patients with L858R/T790M or TKI resistance. Even with osimertinib's advances against L858R/T790M, resistance remains a major challenge. Promising future directions include combination therapies, novel TKIs, and tailored precision strategies [15].

Plants from the Narcissus genus have been utilized in traditional Asian medicine for cancer treatment since the eighteenth century [16]. Narciclasine (Ncs), alternatively called lycoricidinol, was initially extracted in 1967 from bulbs of various Narcissus species in the Amaryllidaceae family during screening for growth inhibitors [17]. As a cytotoxic alkaloid, Ncs possesses documented antitumor and anti-inflammatory effects [18]. It exerts cytotoxicity in lymphoma by inducing cell cycle arrest [19]. In triple-negative breast cancer, Ncs suppresses proliferation and triggers autophagy-mediated apoptosis via AMPK/ULK1 activation. In glioblastoma multiforme, Ncs hinders proliferation and invasion in vitro through actin polymerization, cofilin inactivation, and loss of cell polarity [20]. Notably, the structurally related alkaloid lycorine from Amaryllidaceae interacts with EGFR in docking simulations, inhibits its activity, and thereby suppresses glioblastoma [21]. These observations suggest Ncs as a potential novel TKI effective against mutation-bearing NSCLC.

In the present work, we identified Ncs as an agent capable of suppressing EGFR-dependent NSCLC progression. We showed that Ncs exerts anticancer activity in NSCLC lines expressing either wild-type EGFR or L858R/T790M-EGFR, inhibiting proliferation and promoting cell death. Strikingly, H1975 cells with L858R/T790M-EGFR exhibited far greater sensitivity to Ncs-mediated growth inhibition than wild-type EGFR lines. Computational docking revealed probable binding of Ncs to L858R/T790M-EGFR. In vitro kinase assays confirmed selective inhibition of L858R/T790M-EGFR activity by Ncs. Furthermore, Ncs markedly diminished tumor-like phenotypes in a C. elegans model driven by L858R/T790M-EGFR expression. Consistent antitumor efficacy was observed in mouse xenograft models, positioning Ncs as a candidate therapy for lung cancer control.

Materials and Methods

Materials

Primary antibodies targeting total EGFR (#4267, Cell Signaling Technology (CST)), CDK1 (#9116, CST), phospho-EGFR Y1068 (#44-788 G, Invitrogen), total STAT3 (#4904, CST), phospho-STAT3 Y705 (#9145, CST), phospho-Src (#6943, CST), total-Src (#2109, CST), phospho-CDK1 Y15 (#4539, CST), phospho-Wee1 (#4910, CST), Myt1 (#4282, CST), p21 (#2947, CST), Cdc25B (#9525, CST), GAPDH (#5174, CST), β-actin (#A700-057, Bethyl Laboratory), phospho-ERK1/2 (#9101, CST), Bcl-2 (#sc-7382, Santa Cruz), and c-Myc (#sc-789, Santa Cruz) were employed for Western blotting. Horseradish peroxidase (HRP)-linked anti-rabbit IgG and HRP-linked anti-mouse IgG were sourced from Enzo Life Sciences (Farmingdale, NY). Gefitinib, osimertinib, cycloheximide (CHX), MG132, and propidium iodide (PI) were purchased from Sigma-Aldrich Corporation (St. Louis, MO).

Cell culture

Normal Human Bronchial/Tracheal Epithelial Cells (NHBE) were procured from Lonza (Basel, Switzerland). The non-small cell lung cancer (NSCLC) lines A549, H1299, PC-9, and H1975 were obtained from the American Type Culture Collection (ATCC, Rockville,

MD). NHBE cells were grown in BEGM medium with added growth supplements (Lonza). A549, H1299, PC-9, and H1975 cells were cultured in RPMI medium (Hyclone, Logan, UT) containing 10% FBS (Hyclone, Logan, UT), 100 units/mL penicillin, and 100 µg/mL streptomycin (Thermo Scientific, Waltham, MA). Gefitinib-resistant PC-9-GR cells were developed by gradual exposure of parental PC-9 cells to escalating gefitinib doses, following established protocols [22]. PC-9-GR cells were routinely maintained with 1 µM gefitinib.

Growth curve determination

Cells were seeded into 96-well plates at 4 × 103 cells/well and exposed to varying concentrations of Ncs for 48 hours at 37 °C in a 5% CO_2 humidified incubator. Cell proliferation was tracked with the LionHeart FX automated microscope (Agilent Technologies, Santa Clara, CA). Growth curves and IC50 values were calculated via the logistic growth model, while doubling time (DT) was derived from the formula DT = (ln2/K) (with K determined by the software), all processed using GraphPad software (New York, NY).

Cell viability assay

Cells were seeded in culture dishes and exposed to Ncs for 24 or 48 hours. Viability was evaluated through trypan blue exclusion and the Live/Dead assay kit. In trypan blue staining, detached cells were mixed with 0.2% trypan blue, and live/dead cells were enumerated [23]. For the Live/Dead assay, cells were incubated with 1 µM PI and 1 µM Calcein AM (Invitrogen) for 30 minutes at 37 °C, then imaged via Axio Observer Z1 fluorescence microscopy (Carl Zeiss Microimaging, Thornwood, NY). For the WST-1 assay [24], cells were placed in 96-well plates (5 × 103 cells/well), allowed to attach for 24 hours, then treated with specified Ncs doses and durations. Post-treatment, 10 µL WST-1 reagent (Sigma-Aldrich) was added per well, followed by 2-hour incubation at 37 °C. Optical density was recorded on a Biotek microplate reader (Winooski, VT).

Apoptosis assay

After treatment, cells were collected, incubated with 5 µg/mL PI and 2.5 µg/mL FITC-conjugated annexin V in binding buffer, and subjected to flow cytometric analysis. Results were processed with Cell Quest Software (BD Biosciences, Franklin Lakes, NJ).

Cell cycle analysis

Cells exposed to Ncs for designated periods were fixed overnight in ice-cold 70% ethanol at 4 °C, then stained with propidium iodide (PI) for 30 minutes at room temperature. Cell cycle profiles were assessed using a FACSCalibur flow cytometer (BD Biosciences, Franklin Lakes, NJ).

3D culture assay

A549 and H1975 cells were plated in 8-well chamber slides (Nunc™ Lab-Tek™, Thermo Fisher Scientific, Waltham, MA) at 2 × 103 cells in 300 µL of 5% Matrigel overlaid on a 100 µL 100% Matrigel base layer. Cultures were maintained for 6 days at 37 °C in 5% CO_2, with spheroid images acquired on an Axio Observer Z1 fluorescence microscope (Carl Zeiss Microimaging, Thornwood, NY). Spheroid sizes were measured using the Gen3.1 software (Zeiss).

Immunofluorescence microscopy imaging

Cells grown on coverslips were fixed in 4% paraformaldehyde for 15 minutes at room temperature, permeabilized with Triton X-100, and blocked in 5% BSA. Primary antibodies were applied overnight at 4 °C, followed by washing and incubation with Alexa 488- and 568-conjugated secondary antibodies. Nuclei were counterstained with 0.5 µg/mL DAPI and examined under a Carl Zeiss fluorescence microscope (Gottingen, Germany).

RNA isolation and quantitative real time PCR

Total RNA was isolated using GeneAll kit (Seoul, Korea), and 1 µg was reverse-transcribed to cDNA with the iScript cDNA Synthesis Kit (Bio-Rad, Hercules, CA). Real-time quantitative PCR was conducted on a Roche LightCycler® 96 instrument using SYBR-GREEN master mix (Roche, Basel, Switzerland). Expression levels were normalized to GAPDH via the comparative Ct approach. Primer sequences were: human EGFR forward 5'-ACTGCTGCCACAACCAGTG-3', reverse 5'-GGCTTCGTCTCGGAATTTG-3'; human GAPDH forward 5'-TCTCTGCTCCTCCTGTTC-3', reverse 5'-CGCCCAATACGACCAAAT-3'.

Xenograft model

Subcutaneous implantation of 5 × 106 A549 or H1975 cells was performed in BALB/c nude mice. Upon tumors reaching 30 mm^3, intraperitoneal administration of vehicle or Ncs at 2 mg/kg was conducted thrice weekly.

Tumor size was determined caliper-based, using the equation 1/2(length × width²). Animal procedures were sanctioned by the IACUC of the National Cancer Center Research Institute (NCCRI), an AAALAC International-accredited institution compliant with ILAR standards.

Immunohistochemical staining

Excised tumors were immersed in 10% neutral buffered formalin, processed into paraffin blocks, and sliced to 4 µm thickness. Prior to staining, sections were baked at 56 °C for 1 hour. Automated immunohistochemistry utilized the Discovery XT platform (Ventana Medical Systems, Tucson, AZ, USA). Tissue processing involved deparaffinization and rehydration via EZ Prep (Ventana), followed by buffer rinses. Epitope unmasking occurred through heating in Tris-EDTA (pH 8.0, CC1 solution, Ventana) at 90 °C for 30 minutes. Primary antibody exposure included anti-EGFR (1:100; CST), anti-phospho-EGFR (Y1068), and anti-phospho-STAT3 (1:200; CST). Control sections received non-immune IgG substitution. Examination and photography were done on a Leica light microscope (Wetzlar, Germany) equipped with LAS imaging software.

C. elegans experiments

Standard wild-type and jgIs25 strains were propagated on NGM agar plates at 20 °C. For treatment, jgIs25 worms were raised on plates containing 0.5% DMSO, 2 µM gefitinib, or 2 µM Ncs, with assessment at adulthood. High-resolution imaging involved immobilizing worms in M9 buffer supplemented with 2 mM levamisole (Sigma, L9756) on 2% agarose pads, followed by differential interference contrast microscopy on an Axio A1 system (Zeiss, Jena, Germany). Digital capture employed an Axiocam 705 mono camera (Zeiss). Polyp-bearing individuals were tallied across three plates per group using a stereomicroscope. Replicates exceeded three and yielded reproducible patterns.

Molecular docking

In silico binding analyses were conducted with AMDock software version 1.5.2, and structures were rendered using PyMOL 2.3.2 (Schrödinger, USA). Docking employed diverse PDB entries: wild-type EGFR (1XKK, 6JRK, 6JXT, 7B85, 7U99); double-mutant L858R/T790M-EGFR (3W3O, 3W2P, 3W2Q, 3W2R, 4RJ4, 4RJ5, 4RJ6, 4RJ7, 4RJ8, 5EDQ, 5EDR, 5y25, 7OXB); and an AlphaFold2-computed structure for exon 19 deletion EGFR.

EGFR kinase assay

Enzymatic function was quantified via the ADP-Glo™ system (Promega, Madison, WI), monitoring ADP formation. Assays adhered to supplier guidelines. Reactions comprised kinase buffer, 1 mM ATP, and 20 ng recombinant protein (wild-type or L858R/T790M-EGFR; BPS Bioscience, San Diego, CA) in 20 µL total volume. After 30-minute incubation at 30 °C, residual ATP was exhausted using ADP-Glo™ reagent. Detection mixture then reconverted ADP to ATP, generating luminescence via luciferase reaction proportional to activity. Readings were taken on a Centro LB 96 luminometer (Promega) with 1-second exposure.

Statistical analysis

Datasets underwent an unpaired Student's t-test or a two-way ANOVA with Bonferroni correction. Thresholds for significance were $p < 0.05$ and $p < 0.01$. Presented figures denote means ± standard deviations across three distinct experiments. Graphical data include error bars reflecting standard deviations from triplicate independent runs.

Results and Discussion

Impact of Ncs on proliferation in NSCLC lines

Ncs ($C_{14}H_{13}NO_7$), alternatively termed lycoricidinol, represents a potent alkaloid extracted from Narcissus species **(Figure 1a)** and has demonstrated antiproliferative activity against multiple tumor types [18]. We investigated the growth-suppressive potential of Ncs in several human lung carcinoma models (A549, H1299, H1975) alongside non-malignant bronchial epithelial cells (NHBE) through real-time label-free monitoring via Lionheart automated imaging. Whereas A549 and H1299 harbor wild-type EGFR, H1975 carries the L858R/T790M double mutation responsible for gefitinib resistance [25]. Ncs markedly curtailed proliferation across NSCLC lines in a concentration-dependent fashion while exerting negligible influence on NHBE expansion **(Figure 1b).** Strikingly, H1975 exhibited heightened vulnerability, displaying IC50 values of 22 nM versus 110 nM for A549 and 88 nM for H1299, underscoring preferential sensitivity in the mutant context **(Figures 1c)**. Furthermore, 25 nM Ncs substantially impaired spheroid formation in three-dimensional cultures of both A549 and H1975, a system more reflective of physiological tumor conditions, with

H1975-derived structures appearing considerably reduced in size **(Figures 1f and 1g).** Collectively, these observations reveal robust antineoplastic action of Ncs against NSCLC, most pronounced in cells bearing the gefitinib-refractory L858R/T790M-EGFR alteration.

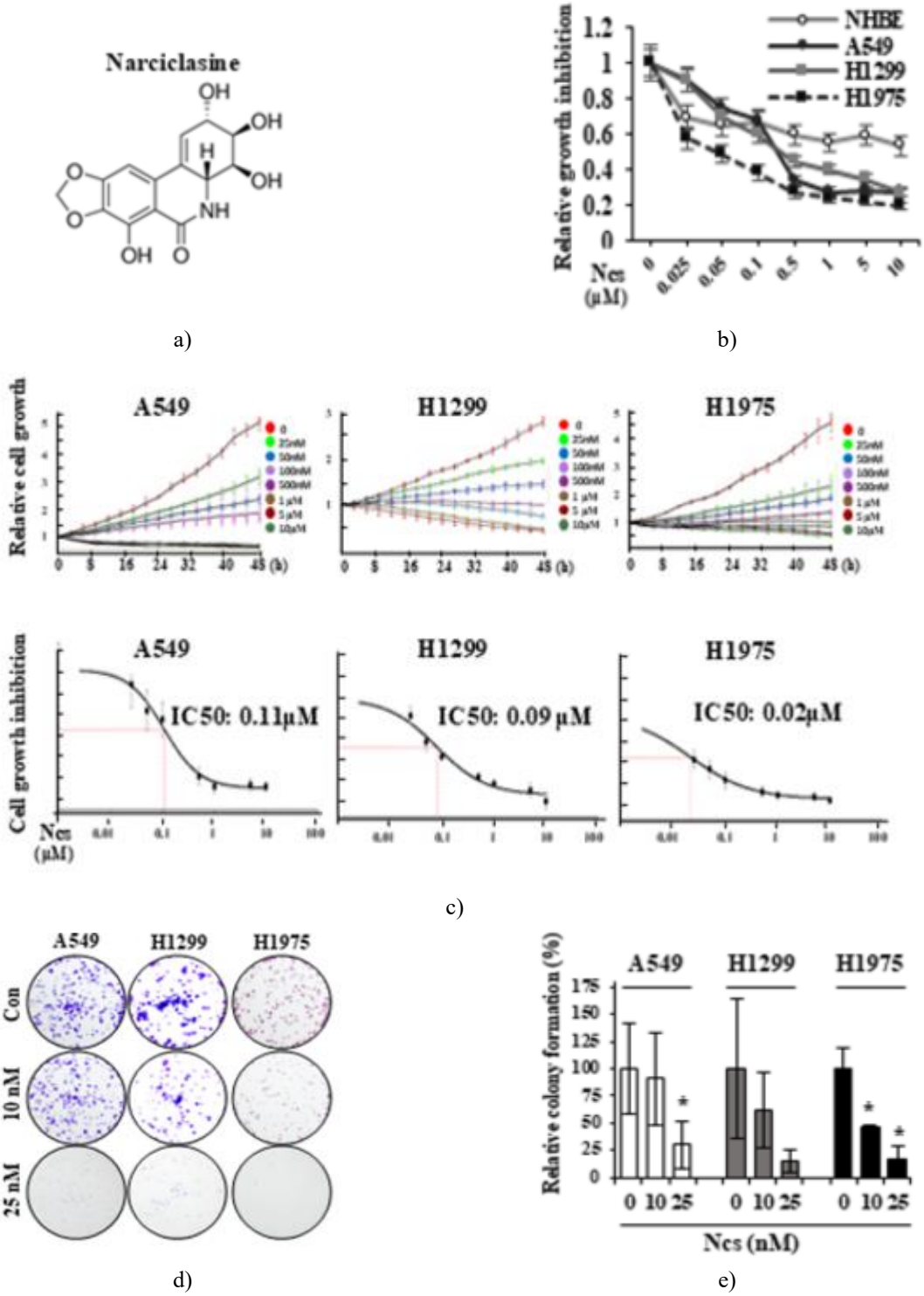

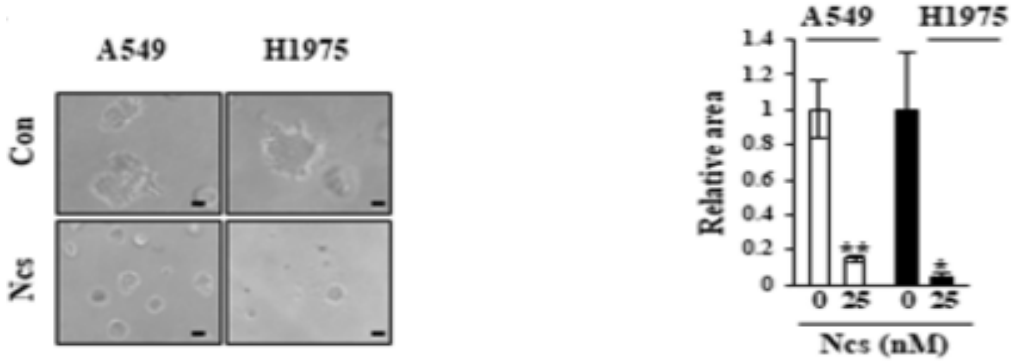

f) g)

Figure 1. Influence of Ncs on proliferation dynamics in NSCLC models. (a) Molecular structure of narciclasine (Ncs). (b) NHBE, A549, H1299, and H1975 cultures received varying Ncs doses (0–10 μM) over 48 h, with proliferation kinetics captured via LionHeart FX automated imaging per protocol. (c) Exposure to graded Ncs levels across specified durations; proliferation assessed as in (b), with IC50 derivation performed using Gen5 software (Biotek). (d and e) Seeding at 3 × 103 cells/well in 6-well formats, followed by 5-day Ncs exposure at indicated doses and subsequent 0.5% crystal violet staining. Representative photographs acquired (d), followed by densitometric quantification across triplicate regions for relative stain intensity (e). (f and g) Placement of 2 × 103 cells within 300 μl 5% Matrigel atop fully coated 8-well chambers, treated with specified Ncs concentrations per detailed protocol. Following a 7-day culture, micrographs obtained (f), and spheroid dimensions were computed from three separate fields (g). Scale bar = 50 μm. Findings replicated across three independent runs. Error bars denote standard deviations from triplicate determinations, *$p < 0.05$, **$p < 0.01$

Influence of Ncs on programmed cell death and cycle progression in NSCLC models

The observed suppression of proliferation by Ncs may arise from the induction of cytotoxicity and/or cycle blockade. Live/dead staining indicated elevated dead fractions (red fluorescence) concomitant with reduced viable populations (green) in both A549 and H1975 upon Ncs exposure **(Figure 2a).** Annexin V/PI-based flow cytometry confirmed apoptotic engagement in each line, without substantial disparity between them **(Figure 2b).** Notably, cycle profiling disclosed profound G2/M accumulation triggered by Ncs, predominantly in H1975 relative to minimal shifts in A549 **(Figure 2c).** Given the L858R/T790M alteration in H1975, we probed Ncs impact on mutant receptor status. Treatment diminished phospho-EGFR signal alongside total EGFR abundance primarily in H1975, with limited changes in A549 **(Figure 2d)**. Correspondingly, downstream ERK1/2 phosphorylation declined preferentially in H1975 **(Figure 2d)**, a key mediator of EGF-driven survival, expansion, and mitotic control [26, 27]. Thus, Ncs appears to impair EGFR functionality and stability, thereby dampening canonical pathway activation.

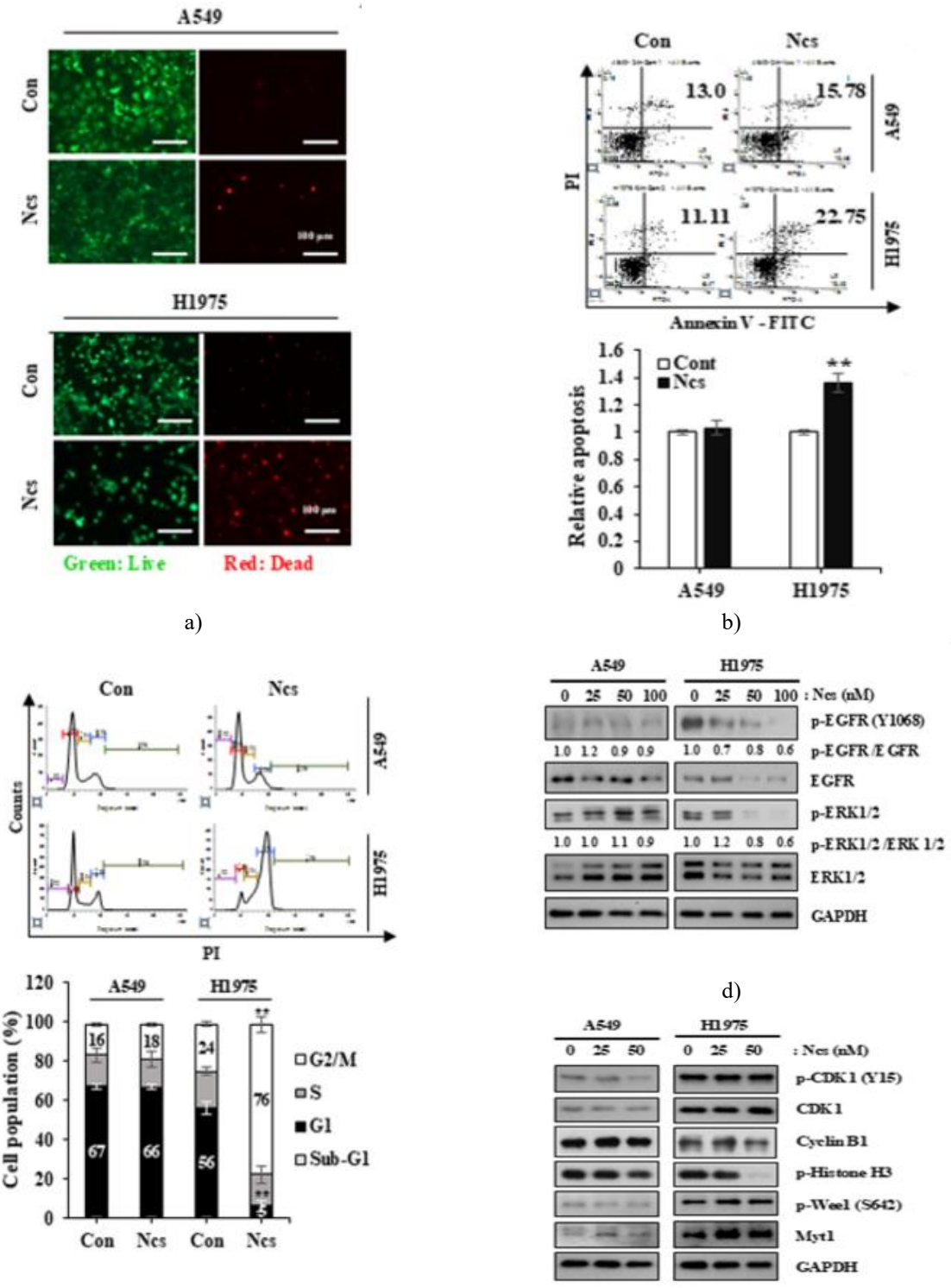

Figure 2. Influence of Ncs on programmed cell death and mitotic progression. (a) Exposure to 50 nM Ncs for 24 h, followed by calcein-AM/PI staining and fluorescence imaging (green indicates viable cells, red denotes necrotic/dead cells), scale bars = 50 μm. (b) After 24 h treatment with 50 nM Ncs, annexin V/PI labeling was performed prior to flow cytometry to assess apoptosis, with quantification combining early and late apoptotic fractions. (c) Cell cycle profiling involved fixation of 50 nM Ncs-exposed cells in 70% ethanol, PI staining, and

subsequent flow cytometric evaluation. (d and e) Cultures received graded doses (0–100 nM) of Ncs for 24 h, and lysates underwent Western blotting with specified antibodies. Band intensities for p-EGFR and p-ERK1/2 were densitometrically normalized to respective total proteins (d). Values reflect averages from three separate runs, with error bars showing standard deviations. *p < 0.05, **p < 0.01

Additional exploration targeted Ncs modulation of G2/M regulatory components, encompassing CDK1, cyclin B1, and phosphorylated Histone H3 **(Figure 2e).** CDK1 remains suppressed during interphase via Tyr15 phosphorylation mediated by inhibitory kinases Wee1 and Myt1. Toward late G2, cyclin B1 buildup deactivates these restraints, promoting mitotic entry [28]. Aurora kinase- or ERK1/2-driven Ser10 phosphorylation of Histone H3 facilitates chromosomal condensation essential for mitosis [29], while EGF signaling through RAS-MAPK-ERK1/2 cascade supports this modification for mitotic advancement [30]. Ncs exposure lowered cyclin B1 abundance, elevated phospho-Wee1 and Myt1, thereby sustaining CDK1 inhibitory phosphorylation, and reduced Histone H3 phosphorylation **(Figure 2e).** Overall, these alterations demonstrate Ncs blockade of G2/M transition via disruption of critical mitotic controllers, culminating in cycle arrest. Notably, such molecular shifts were far more evident in H1975 than in A549, consistent with pronounced G2/M accumulation in the gefitinib-refractory L858R/T790M-bearing line [12].

Impact of Ncs on proliferation in PC-9 and PC-9-GR models

To ascertain Ncs efficacy against gefitinib-refractory NSCLC, we utilized PC-9 (exon 19 deletion E746–A750, gefitinib-sensitive [31]) and derived PC-9-GR (acquired resistance via chronic exposure; **Figure 3a**). Ncs suppressed expansion in both lines concentration-dependently, as evidenced by WST-1 metabolic readout **(Figure 3b)** and reduced confluency under phase microscopy **(Figure 3c).** Cytotoxicity was enhanced in PC-9-GR, with greater dead cell enrichment **(Figure 3d)** and sharper viable fraction decline**.** Cycle distribution showed Ncs provoking G1 plus G2/M blockade in PC-9, versus S and G2/M in PC-9-GR **(Figures 3e and 3f).** Elevated doses similarly augmented G2/M in A549**,** yet preferential G2/M engagement emerged in TKI-resistant contexts like H1975 and PC-9-GR **(Figures 2c and 3f).**

Acquired TKI resistance involves EGFR-reliant (secondary mutations) or bypass mechanisms, notably STAT3/Src hyperactivation [32-34]. Sequencing confirmed the absence of additional EGFR alterations in PC-9-GR, implicating independence from EGFR. Baseline EGFR protein was higher in resistant cells, though phospho-EGFR favored sensitive PC-9; conversely, p-STAT3 and p-Src dominated in PC-9-GR, aligning with bypass signaling reports [33, 34]. Ncs diminished total and activated EGFR selectively in PC-9, whereas it potently abrogated p-STAT3 and p-Src in PC-9-GR **(Figure 3g)**, implying suppression of alternate survival axes underlies growth restraint in this resistant subset. Despite distinct mutational profiles, both resistant lines (H1975, PC-9-GR) displayed comparable Ncs vulnerability down to 10 nM**.**

Ncs modulation of EGFR turnover and function

In H1975, Ncs elicited concentration- **(Figure 2d)** and duration-dependent **(Figure 4a)** declines in total and phospho-EGFR. Paradoxically, EGFR transcripts rose **(Figure 4b),** pinpointing posttranscriptional control. Cotreatment with translation inhibitor cycloheximide (CHX) accelerated EGFR loss beyond CHX alone **(Figure 4c),** confirming abbreviated protein lifespan. Proteasome blockade (MG132) and autophagy-lysosome inhibition (BafA1) each mitigated degradation **(Figure 4d)**, evidencing dual proteasomal/lysosomal routing. Confocal analysis showed basal diffuse EGFR shifting to LAMP1 colocalization post-Ncs **(Figure 4e)**, supporting lysosomal involvement. Furthermore, Ncs blunted both ligand-stimulated and constitutive EGFR phosphorylation **(Figure 4f).** Collectively, Ncs promotes EGFR inactivation and clearance via combined degradative machineries.

Effects of Ncs on wild-type EGFR and L858R/T790M-EGFR function

Lycorine, a structurally related isocarbostyril alkaloid, was previously shown to engage wild-type EGFR in computational docking [21]. Given Ncs-mediated EGFR suppression and proliferation restraint across NSCLC models—A549 (wild-type EGFR), H1975 (L858R/T790M-EGFR), and PC-9 (exon 19 deletion EGFR) **(Figures. 1–3)**—we performed in silico docking against multiple PDB structures to probe Ncs-EGFR interactions. Binding poses varied considerably across wild-type and mutant forms, yet calculated affinities remained comparable (7.2~8.4 kcal/mol). Predominant forces appeared hydrophobic and van der Waals across

both wild-type and double-mutant EGFR, overshadowing hydrogen bonding **(Figure 5a).** Specifically, Ncs engaged 16 residues in wild-type EGFR, 18 in L858R/T790M-EGFR, and 16 in the exon 19 deletion variant, with differing residue identities. The exon 19 deletion (E746–A750) structure was predicted via AlphaFold due to the absence of experimental coordinates. Hydrogen bonding predictions yielded five contacts in the deletion mutant (Glu758, Arg836—potentially triple-bonded—and Tyr869), versus one each in wild-type (Ser720) and L858R/T790M (Asn842). Overall, these simulations support the physical interaction of Ncs with both wild-type and mutated EGFR isoforms.

To assess direct kinase inhibition, purified wild-type EGFR and L858R/T790M-EGFR were subjected to in vitro ADP-Glo assays. Gefitinib potently blocked wild-type activity while sparing the double mutant **(Figure 5b),** recapitulating established resistance [25]. Osimertinib, engineered against T790M-containing EGFR [35], robustly inhibited both variants. Notably, Ncs mildly curtailed wild-type EGFR catalysis but markedly attenuated L858R/T790M-EGFR function, though less potently than osimertinib. These findings confirm Ncs as a binder and inhibitor of EGFR kinase, exhibiting selectivity toward the resistant mutant in cell-free conditions.

In vivo antitumor activity of Ncs

Antineoplastic potential was evaluated in the C. elegans jgIs25 strain engineered to express human L858R/T790M-EGFR [36]. Relative to wild-type nematodes, jgIs25 displays ventral polyps manifesting as a multivulva (Muv) phenotype, modeling oncogenesis **(Figure 6a)** [36]. Exposure to 2 μM gefitinib failed to alter polyp incidence versus vehicle **(Figure 6b).** Conversely, 2 μM Ncs halved Muv-positive individuals and polyp counts **(Figures 6b and 6c).** In mammalian xenografts, BALB/c nude mice received subcutaneous A549 or H1975 implants, followed by thrice-weekly intraperitoneal DMSO or Ncs over 27 (A549) or 17 (H1975) days. Ncs cohorts exhibited delayed volume expansion and reduced final tumor mass in both models **(Figures 6d, 6e, 6g and 6h).** Tissue immunostaining demonstrated diminished EGFR, phospho-EGFR, and phospho-STAT3 abundance in treated tumors **(Figures 6f and 6i).** Collectively, these observations position Ncs as a candidate agent against lung tumors, efficacious via EGFR-dependent and bypass mechanisms, particularly in gefitinib-refractory contexts **(Figure 7).**

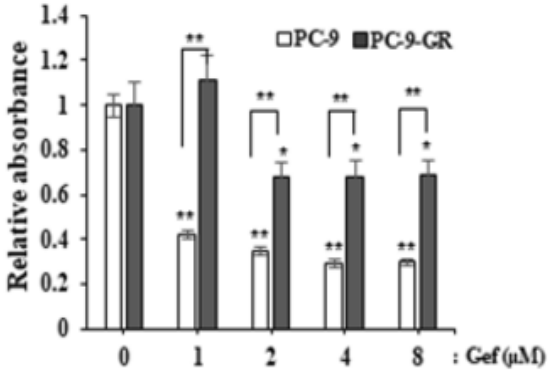

a)

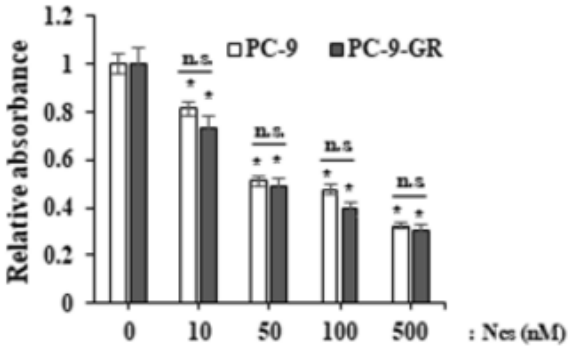

b)

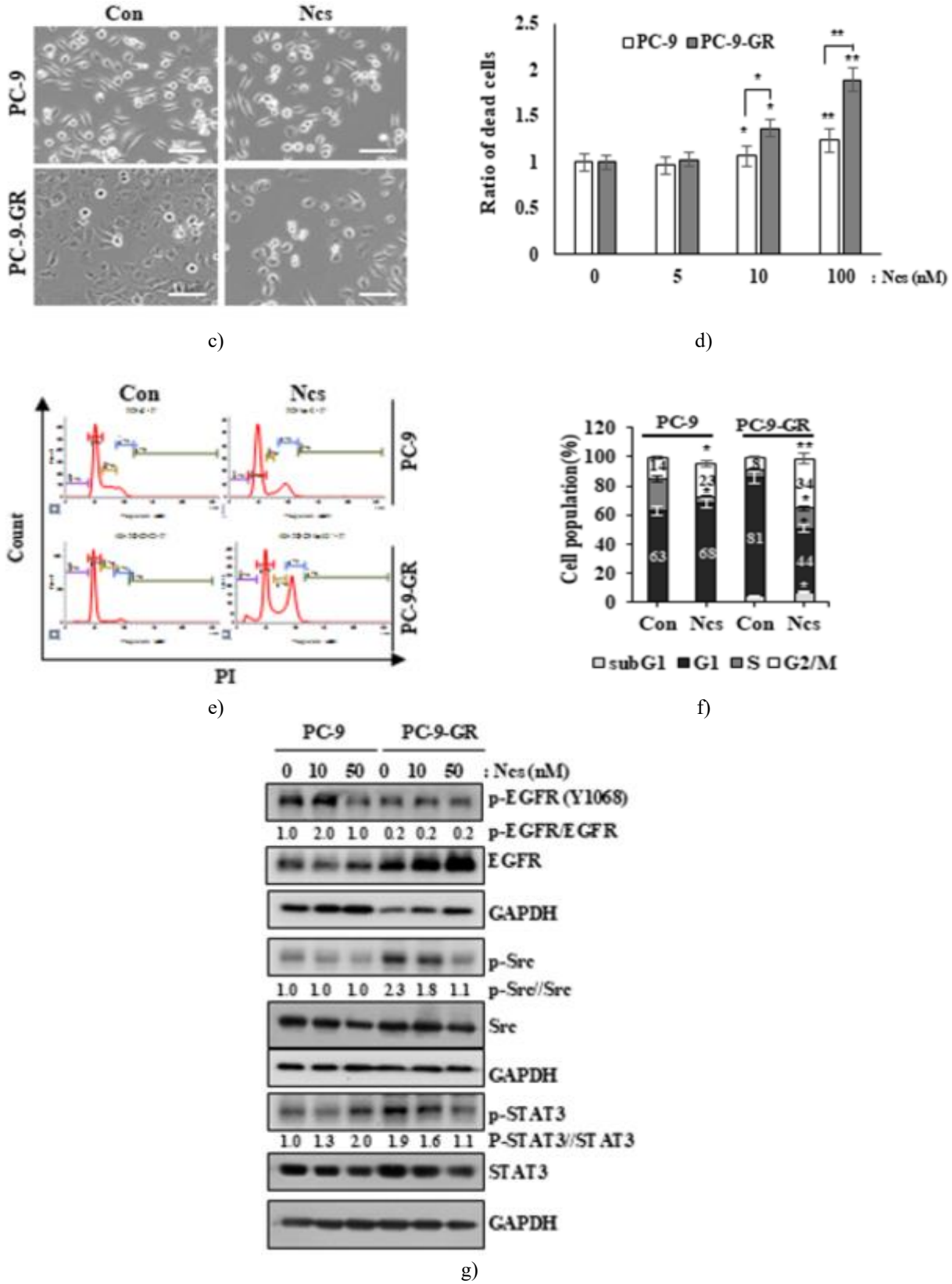

Figure 3. Ncs impact on proliferation in PC-9 and resistant PC-9-GR models. (a) Seeding at 3 × 103 cells/well in 96-well format, followed by graded gefitinib exposure for 48 h. (b) Cultures received specified Ncs doses over 48

hours, with viability quantified via WST-1. (c) Phase-contrast micrographs after 48-hour Ncs treatment. (d) Plating at 1 × 104 cells/well in 24-well dishes, 48 h Ncs exposure at indicated levels, followed by trypan blue enumeration of viable/non-viable fractions. (e and f) Post-48 h Ncs, ethanol fixation, PI labeling, and flow cytometric cycle profiling. (g) Treatment with 0-50 nM Ncs for 24 h in PC-9 and PC-9-GR, lysates were immunoblotted with designated antibodies. Densitometry of p-EGFR, p-Src, and p-STAT3 normalized to respective totals. Averages derived from triplicate experiments, error bars indicate standard deviations across three replicates. Magnification: x 100, n.s. >0.05, *P < 0.05, **P < 0.01

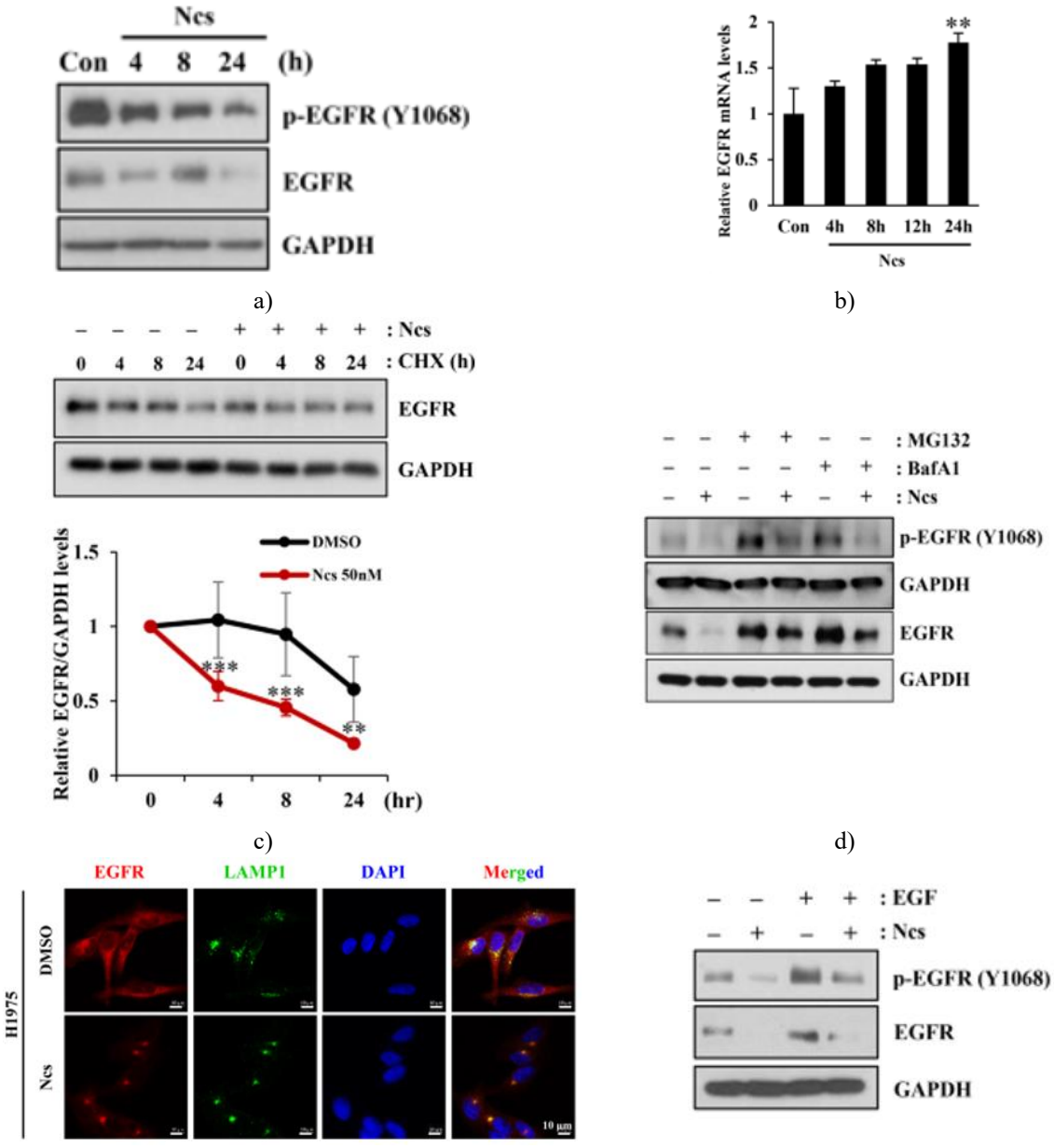

Figure 4. Ncs influence on EGFR function and downstream pathways. (a) Exposure of H1975 cultures to 50 nM Ncs across specified durations, followed by lysate preparation and Western blotting with designated antibodies. (b) Following 50 nM Ncs treatment for the indicated periods, RNA extraction was performed. EGFR transcript abundance was quantified via quantitative RT-PCR, with normalization against GAPDH. (c) Administration of 20

μM cycloheximide (CHX) at the listed intervals, combined with either vehicle or 50 nM Ncs over 24 h. Lysates underwent immunoblotting with relevant antibodies (upper section). Densitometric analysis of EGFR bands, normalized to GAPDH, compared CHX effects under vehicle versus Ncs conditions (lower section). (d) Cotreatment with 50 nM Ncs for 24 h alongside BafA1 (20 nM, final 12 h) or MG132 (20 μM, final 2 h). Resulting lysates were probed by Western blot with specified antibodies. (e) Coverslip-grown cells received vehicle or 50 nM Ncs for 24 h, followed by 4% paraformaldehyde fixation and immunofluorescent labeling for DAPI, EGFR, and LAMP1. (f) Preincubation with 50 nM Ncs for 24 h, then acute EGF challenge (10 nM, 15 min). Lysates were analyzed via immunoblotting with targeted antibodies. Findings are consistent across three separate runs. Error bars denote standard deviations from triplicate assessments, *P < 0.05, **P < 0.01, ***P < 0.001

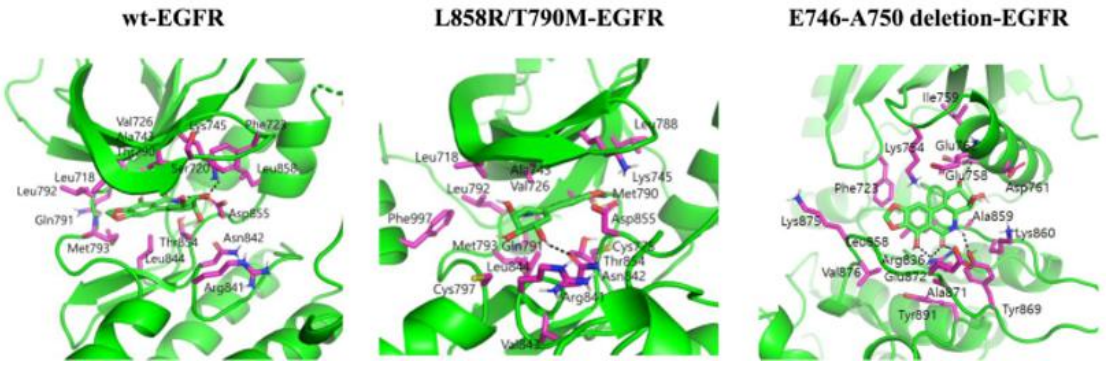

a)

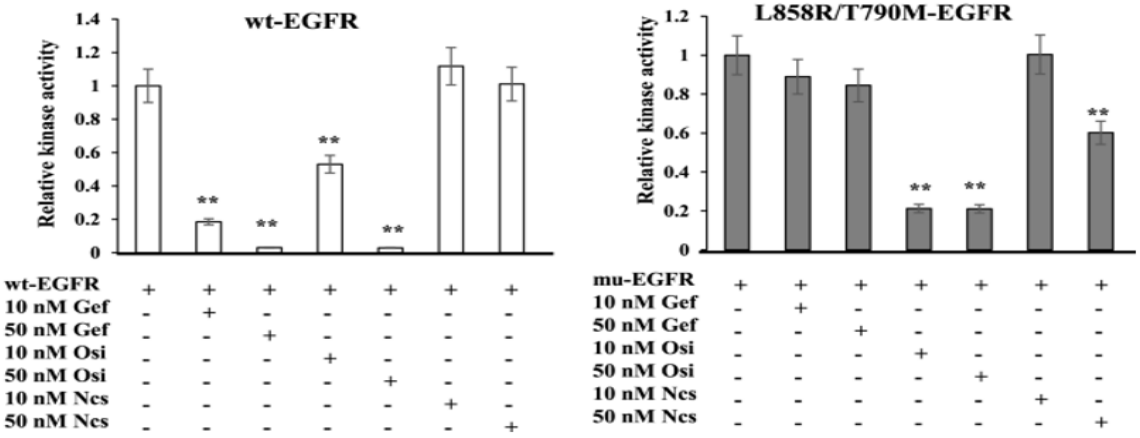

b)

Figure 5. Computational binding and enzymatic inhibition of EGFR by Ncs. (a) In silico docking outcomes depicting Ncs engagement with wild-type, L858R/T790M, and E746-A750 deletion EGFR variants. Interacting amino acids are highlighted in magenta, and potential hydrogen bonds are indicated by dashed lines. (b) Assessment of Ncs impact on EGFR catalysis via ADP-Glo platform. Recombinant 20 ng wild-type or mutant EGFR was exposed to Ncs, gefitinib (established inhibitor), or osimertinib (third-generation agent). Reproducible across three independent assays. Error bars reflect standard deviations from three replicates, *P < 0.05, **P < 0.01

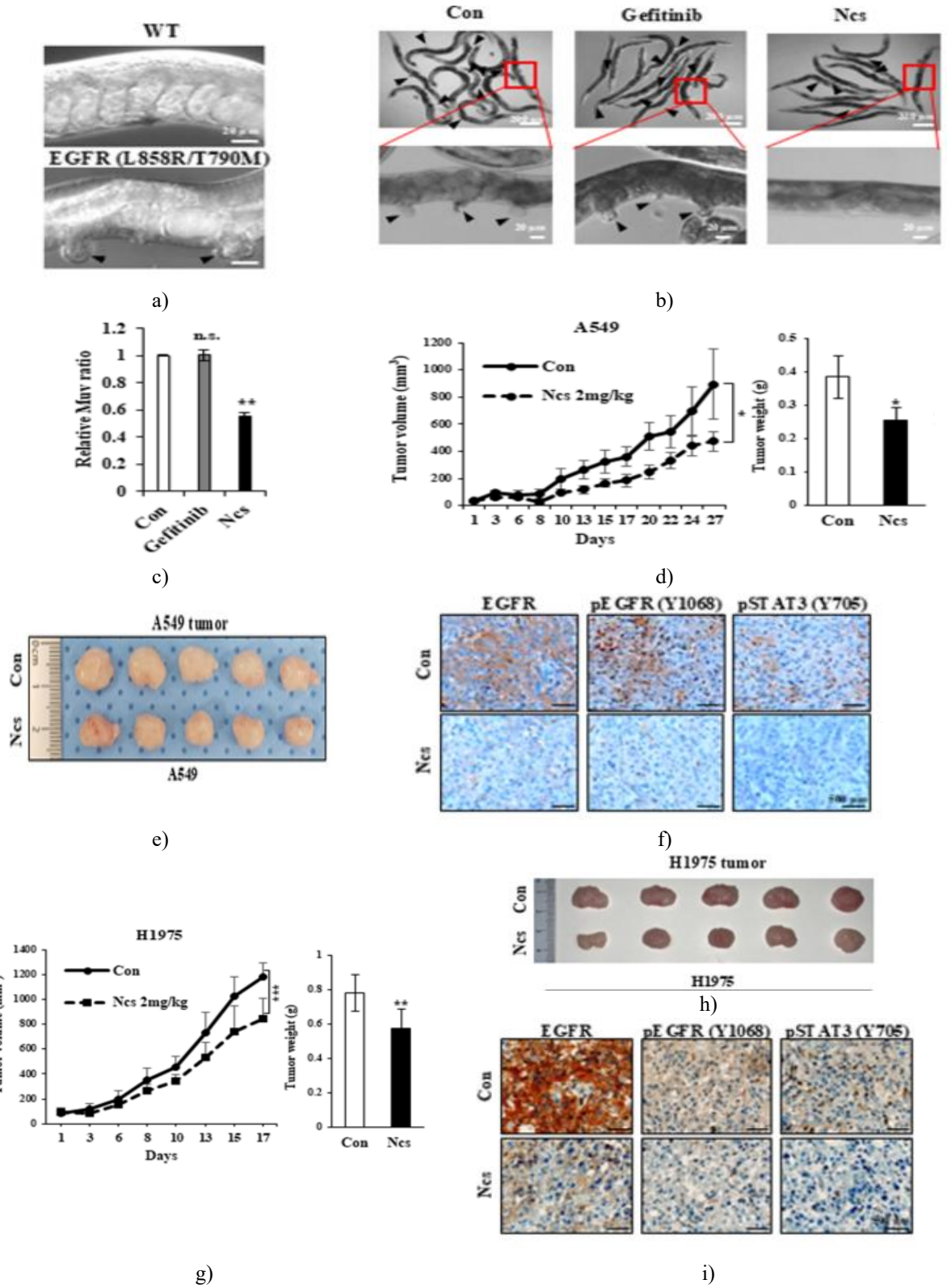

Figure 6. In vivo antineoplastic activity of Ncs. (a) Mature C. elegans specimens: wild-type (WT) versus jgIs25 strain. Ventral polyp formation in jgIs25 is marked by arrows (lower panel). Scale bar = 20 μm. (b) Response of jgIs25 to gefitinib or Ncs exposure. Upper panel arrows denote polyps; the boxed region is enlarged below. Scale

bar = 200 µm (upper), 20 µm (lower). (c) Polyp incidence quantification in drug-exposed jgIs25 cohorts. (d and g) Xenograft progression in nude mice bearing subcutaneous A549 or H1975 implants under control or Ncs regimen. Serial volume recordings are shown, with terminal mass determination post-euthanasia. (e and h) Photographic documentation of excised tumors. (F and I) Immunoperoxidase staining of tumor sections employing antibodies against EGFR, phospho-EGFR (Y1068), and phospho-STAT3 (Y705). Scale bar = 500 µm. Observations replicated in three distinct studies. Error bars indicate standard deviations across triplicate measurements, *p < 0.05, **p < 0.01, *p < 0.001

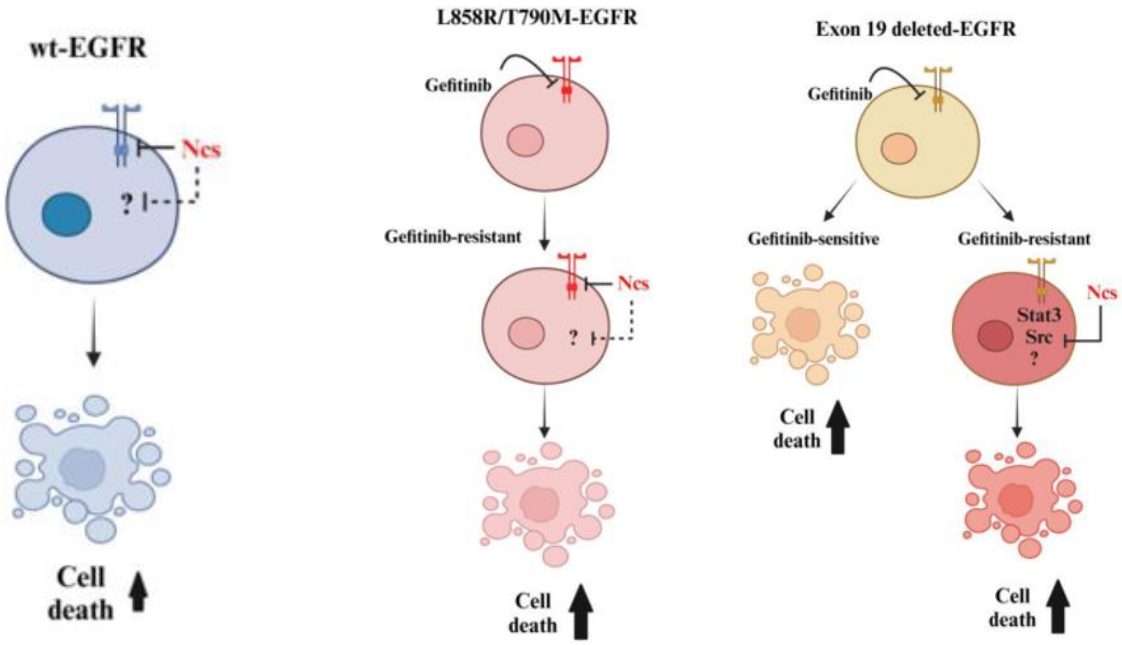

a) b) c)

Figure 7. Ncs-triggered cytotoxicity in NSCLC models with varying EGFR genotypes. (a) In cells with wild-type EGFR (wt-EGFR), Ncs promotes cell death via EGFR blockade or additional unidentified routes (marked by "?"). (b) In cells carrying the gefitinib-refractory L858R/T790M EGFR variant, Ncs drives cytotoxicity through direct EGFR suppression and/or interference with bypass signaling. (c) Cells featuring exon 19-deleted EGFR exhibit initial gefitinib responsiveness but may acquire resistance over time; nonetheless, such resistant populations remain vulnerable to Ncs primarily via STAT3 and Src pathway disruption.

This investigation establishes that Ncs, derived from Narcissus species, potently curtails proliferation in lung carcinoma cells harboring EGFR alterations that confer resistance to the EGFR-TKI gefitinib, positioning Ncs as a viable alternative agent for managing TKI-resistant NSCLC.

Ncs and lycorine share a common crinine-type scaffold, characterized by a perhydroindole-pyrrolidine fused ring system [18]. Prior studies have documented lycorine's antitumor properties in glioblastoma and predicted its docking to the EGFR kinase domain through hydrogen bonds with Asn842, Lys745, and Thr854 [21]. Given Ncs's superior antiproliferative potency compared to lycorine [19] and its enhanced efficacy in H1975 cells, we evaluated potential interactions with wild-type and mutant EGFR via computational docking. Ncs exhibited binding to both wild-type and variant EGFR forms, predominantly driven by hydrophobic and van der Waals contacts. Hydrogen bonding was also predicted, though the participating residues varied across genotypes due to mutational differences **(Figure 5a).** In vitro kinase assays demonstrated that Ncs more strongly suppressed L858R/T790M-EGFR catalytic activity than wild-type EGFR **(Figure 5b).** Specifically, wild-type EGFR showed minor inhibition at 50 nM Ncs and substantial reduction at 100 nM, whereas the double mutant

experienced significant suppression at 25 nM Ncs, achieving roughly 50% inhibition at 50 nM with limited further decline**.** These findings indicate that L858R/T790M-EGFR requires lower Ncs concentrations for effective kinase inhibition in vitro. Corroborating cellular data, Ncs markedly diminished EGFR signaling in H1975 (L858R/T790M) compared to A549 (wild-type) cells **(Figure 2d).** Proliferation assays further revealed heightened sensitivity in H1975 (IC50 22 nM) relative to A549 (110 nM) and H1299 (88 nM) **(Figure 1b)**. To confirm the role of L858R/T790M-EGFR in conferring Ncs vulnerability, we performed siRNA-mediated knockdown and ectopic expression experiments**.** Introducing L858R/T790M-EGFR into A549 (while silencing wild-type) increased Ncs responsiveness, whereas replacing L858R/T790M with wild-type EGFR in H1975 abolished the heightened sensitivity**.** Thus, Ncs efficacy appears closely tied to the presence of the L858R/T790M mutant.

In A549 cells, 50 nM gefitinib, erlotinib, or Ncs yielded equivalent growth suppression, akin to 10 nM osimertinib. In contrast, H1975 cells were largely unresponsive to gefitinib or erlotinib at similar doses, while Ncs and osimertinib markedly impaired proliferation, with osimertinib displaying slightly superior activity**.** Additionally, 50 nM Ncs provoked robust G2/M accumulation in H1975 but not A549 cells **(Figure 2c),** though elevated concentrations (50–200 nM) induced G2/M blockade in A549 as well. Remarkably, Ncs dose-dependently restricted growth in osimertinib-resistant H1975 derivatives, with an IC50 of 49.7 nM**.** These observations highlight Ncs as a promising therapeutic option for lung cancer patients progressing on osimertinib.

The internalization and degradation of EGFR reduce its presence on the plasma membrane, thus restricting downstream EGFR signaling pathways that are essential for cellular proliferation and survival [37]. Two primary therapeutic approaches exist to inhibit EGFR: monoclonal anti-EGFR antibodies and tyrosine kinase inhibitors (TKIs). Anti-EGFR antibodies attach to the extracellular portion of the receptor, blocking ligand interaction and/or inducing receptor endocytosis and subsequent degradation [38]. For instance, Okada *et al*. showed that an anti-EGFR antibody facilitates EGFR degradation via the endosomal-lysosomal route, a mechanism closely linked to its antitumor efficacy in colorectal cancer cells [39]. EGFR TKIs block the kinase function of the receptor [40], and certain TKIs can additionally promote EGFR degradation. As examples, gefitinib at elevated concentrations was found to lower protein expression of the EGFRvIII mutant [41], while erlotinib therapy reduced EGFR protein amounts in both head and neck cancer patients and cell lines [42]. In the current investigation, Ncs treatment markedly decreased EGFR protein expression, even though EGFR mRNA expression increased **(Figure 4b).** Ncs promoted the co-localization of EGFR with LAMP1 **(Figure 4e),** and the Ncs-mediated reduction in EGFR was prevented by BafA1 and MG132 **(Figure 4d).** Furthermore, Ncs suppressed both constitutive and EGF-induced EGFR phosphorylation **(Figure 4f).** Collectively, these results suggest that Ncs impairs EGFR signaling through direct inhibition of kinase activity as well as by enhancing receptor degradation.

Gefitinib potently suppresses the kinase activity of EGFR harboring exon 19 deletions, and PC-9 cells carrying this mutation exhibit high sensitivity to gefitinib [43]. A gefitinib-resistant PC-9-GR cell line was generated **(Figure 3a)**. As no secondary mutations were detected in the exon 19-deleted EGFR of PC-9-GR cells**,** the acquired resistance seems unrelated to alterations in EGFR itself and probably relies on bypass survival mechanisms. Consistent with this, although total EGFR was higher, phosphorylated EGFR was lower in PC-9-GR cells than in parental PC-9 cells **(Figure 3g).** In contrast, Src and STAT3 phosphorylation were increased in PC-9-GR cells. Treatment with Ncs reduced p-EGFR in PC-9 cells but had no effect on p-EGFR in PC-9-GR cells; however, it diminished p-Src and p-STAT3 levels in the resistant line. Previous work has shown that Ncs exerts anticancer activity via STAT3 suppression and directly interacts with STAT3 in tamoxifen-resistant breast cancer cells [44]. Given that Ncs inhibited proliferation in both PC-9 and PC-9-GR cells, it appears that Ncs restrains cell growth via both EGFR-dependent mechanisms and EGFR-independent routes, including Src and STAT3 pathways.

A C. elegans model expressing L858R/T790M-mutant EGFR was utilized, leading to multivulval phenotypes **(Figure 6a).** Gefitinib failed to reduce multivulva development, confirming resistance. Notably, Ncs substantially suppressed multivulva formation in this model **(Figures 6b and 6c).** Additionally, Ncs displayed robust antitumor activity in mouse xenografts bearing either A549 or H1975 cells **(Figures 6d and 6g).** Ncs administration also lowered EGFR, p-EGFR, and p-STAT3 levels in the excised tumor tissues **(Figure 6i).**

These observations demonstrate that Ncs achieves antitumor effects against NSCLC through combined EGFR kinase blockade and receptor degradation, as evidenced in both in vitro and in vivo settings. Overall, narciclasine warrants further development as a candidate therapy for EGFR-driven lung cancer, especially in tumors harboring gefitinib-resistant mutations.

Conclusion

Non-small cell lung cancer (NSCLC) is frequently propelled by aberrant EGFR activation, and resistance to EGFR-TKIs like gefitinib poses a significant clinical obstacle. Here, we present narciclasine (Ncs) as an effective agent against NSCLC, including cases with TKI-resistant EGFR variants. Ncs targets diverse EGFR forms, triggers cell cycle arrest, and inhibits tumor progression in preclinical systems, outperforming gefitinib in resistant contexts. These results position Ncs as a promising new treatment option—potentially alone or combined with existing EGFR-TKIs—to address resistance in NSCLC.

Acknowledgments: None

Conflict of Interest: None

Financial Support: None

Ethics Statement: None

References

1. Thandra KC, Barsouk A, Saginala K, Aluru JS, Barsouk A. Epidemiology of lung cancer. Contemp Oncol (Pozn). 2021;25(1):45–52.
2. El-Telbany A, Ma PC. Cancer genes in lung cancer: racial disparities: are there any? Genes Cancer. 2012;3(7–8):467–80.
3. Sigismund S, Avanzato D, Lanzetti L. Emerging functions of the EGFR in cancer. Mol Oncol. 2018;12(1):3–20.
4. Rosell R, Moran T, Queralt C, Porta R, Cardenal F, Camps C, Majem M, Lopez-Vivanco G, Isla D, Provencio M, et al. Screening for epidermal growth factor receptor mutations in lung cancer. N Engl J Med. 2009;361(10):958–67.
5. Shigematsu H, Gazdar AF. Somatic mutations of epidermal growth factor receptor signaling pathway in lung cancers. Int J Cancer. 2006;118(2):257–62.
6. Paez JG, Janne PA, Lee JC, Tracy S, Greulich H, Gabriel S, Herman P, Kaye FJ, Lindeman N, Boggon TJ, et al. EGFR mutations in lung cancer: correlation with clinical response to gefitinib therapy. Science. 2004;304(5676):1497–500.
7. Sordella R, Bell DW, Haber DA, Settleman J. Gefitinib-sensitizing EGFR mutations in lung cancer activate anti-apoptotic pathways. Science. 2004;305(5687):1163–67.
8. Gajiwala KS, Feng J, Ferre R, Ryan K, Brodsky O, Weinrich S, Kath JC, Stewart A. Insights into the aberrant activity of mutant EGFR kinase domain and drug recognition. Structure. 2013;21(2):209–19.
9. Huang L, Fu L. Mechanisms of resistance to EGFR tyrosine kinase inhibitors. Acta Pharm Sin B. 2015;5(5):390–401.
10. Mok TS, Wu YL, Thongprasert S, Yang CH, Chu DT, Saijo N, Sunpaweravong P, Han B, Margono B, Ichinose Y, et al. Gefitinib or carboplatin-paclitaxel in pulmonary adenocarcinoma. N Engl J Med. 2009;361(10):947–57.
11. Mitsudomi T, Morita S, Yatabe Y, Negoro S, Okamoto I, Tsurutani J, Seto T, Satouchi M, Tada H, Hirashima T, et al. Gefitinib versus cisplatin plus docetaxel in patients with non-small-cell lung cancer harbouring mutations of the epidermal growth factor receptor (WJTOG3405): an open label, randomised phase 3 trial. Lancet Oncol. 2010;11(2):121–28.
12. Pao W, Miller VA, Politi KA, Riely GJ, Somwar R, Zakowski MF, Kris MG, Varmus H. Acquired resistance of lung adenocarcinomas to gefitinib or erlotinib is associated with a second mutation in the EGFR kinase domain. PLoS Med. 2005;2(3):e73.
13. Vikis H, Sato M, James M, Wang D, Wang Y, Wang M, Jia D, Liu Y, Bailey-Wilson JE, Amos CI, et al. EGFR-T790M is a rare lung cancer susceptibility allele with enhanced kinase activity. Cancer Res. 2007;67(10):4665–70.
14. Leonetti A, Sharma S, Minari R, Perego P, Giovannetti E, Tiseo M. Resistance mechanisms to osimertinib in EGFR-mutated non-small cell lung cancer. Br J Cancer. 2019;121(9):725–37.
15. Ramalingam SS, Vansteenkiste J, Planchard D, Cho BC, Gray JE, Ohe Y, Zhou C, Reungwetwattana T, Cheng Y, Chewaskulyong B, et al. Overall survival with osimertinib in untreated, EGFR-Mutated advanced NSCLC. N Engl J Med. 2020;382(1):41–50.

16. Kornienko A. Evidente a: chemistry, biology, and medicinal potential of narciclasine and its congeners. Chem Rev. 2008;108(6):1982–2014.
17. Ceriotti G. Narciclasine: an antimitotic substance from narcissus bulbs. Nature. 1967;213(5076):595–96.
18. Furst R. Narciclasine - an amaryllidaceae alkaloid with potent antitumor and anti-inflammatory properties. Planta Med. 2016;82(16):1389–94.
19. Gopalakrishnan R, Matta H, Choi S, Chaudhary PM. Narciclasine, an isocarbostyril alkaloid, has preferential activity against primary effusion lymphoma. Sci Rep. 2020;10(1):5712.
20. Lefranc F, Sauvage S, Van Goietsenoven G, Megalizzi V, Lamoral-Theys D, Debeir O, Spiegl-Kreinecker S, Berger W, Mathieu V, Decaestecker C, et al. Narciclasine, a plant growth modulator, activates Rho and stress fibers in glioblastoma cells. Mol Cancer Ther. 2009;8(7):1739–50.
21. Shen J, Zhang T, Cheng Z, Zhu N, Wang H, Lin L, Wang Z, Yi H, Hu M. Lycorine inhibits glioblastoma multiforme growth through EGFR suppression. J Exp Clin Cancer Res. 2018;37(1):157.
22. Terai H, Soejima K, Yasuda H, Nakayama S, Hamamoto J, Arai D, Ishioka K, Ohgino K, Ikemura S, Sato T, et al. Activation of the FGF2-FGFR1 autocrine pathway: a novel mechanism of acquired resistance to gefitinib in NSCLC. Mol Cancer Res. 2013;11(7):759–67.
23. Strober W. Trypan blue exclusion test of cell viability. Curr Protoc Immunol. 2015;111:A3 1–3 3.
24. Ishiyama M, Shiga M, Sasamoto K, Mizoguchi M. He P-G. A new sulfonated tetrazolium salt that produces a highly water-soluble formazan dye. Chem Pharm Bull (Tokyo). 1993;41(6):1118–22.
25. Tam IY, Leung EL, Tin VP, Chua DT, Sihoe AD, Cheng LC, Chung LP, Wong MP. Double EGFR mutants containing rare EGFR mutant types show reduced in vitro response to gefitinib compared with common activating missense mutations. Mol Cancer Ther. 2009;8(8):2142–51.
26. Feng Y, Dai X, Li X, Wang H, Liu J, Zhang J, Du Y, Xia L. EGF signalling pathway regulates colon cancer stem cell proliferation and apoptosis. Cell Prolif. 2012;45(5):413–19.
27. Wee P, Wang Z. Epidermal growth factor receptor cell proliferation signaling pathways. Cancers (Basel) 2017;9(5).
28. Giacinti C, Giordano A. RB and cell cycle progression. Oncogene. 2006;25(38):5220–27.
29. Clayton AL, Mahadevan LC. Map kinase-mediated phosphoacetylation of histone H3 and inducible gene regulation. FEBS Lett. 2003;546(1):51–58.
30. Choi HS, Choi BY, Cho YY, Mizuno H, Kang BS, Bode AM, Dong Z. Phosphorylation of histone H3 at serine 10 is indispensable for neoplastic cell transformation. Cancer Res. 2005;65(13):5818–27.
31. Ono M, Hirata A, Kometani T, Miyagawa M, Ueda S, Kinoshita H, Fujii T, Kuwano M. Sensitivity to gefitinib (Iressa, ZD1839) in non-small cell lung cancer cell lines correlates with dependence on the epidermal growth factor (EGF) receptor/extracellular signal-regulated kinase 1/2 and EGF receptor/Akt pathway for proliferation. Mol Cancer Ther. 2004;3(4):465–72.
32. He J, Huang Z, Han L, Gong Y, Xie C. Mechanisms and management of 3rd-generation EGFR-TKI resistance in advanced non-small cell lung cancer (Review). Int J Oncol. 2021;59(5).
33. Liu Z, Ma L, Sun Y, Yu W, Wang X. Targeting STAT3 signaling overcomes gefitinib resistance in non-small cell lung cancer. Cell Death Dis. 2021;12(6):561.
34. Yoshida T, Zhang G, Smith MA, Lopez AS, Bai Y, Li J, Fang B, Koomen J, Rawal B, Fisher KJ, et al. Tyrosine phosphoproteomics identifies both codrivers and cotargeting strategies for T790M-related EGFR-TKI resistance in non-small cell lung cancer. Clin Cancer Res. 2014;20(15):4059–74.
35. Remon J, Steuer CE, Ramalingam SS. Felip E: osimertinib and other third-generation EGFR TKI in EGFR-mutant NSCLC patients. Ann Oncol. 2018;29(suppl_1):i20–27.
36. Bae YK, Sung JY, Kim YN, Kim S, Hong KM, Kim HT, Choi MS, Kwon JY, Shim J. An in vivo C. elegans model system for screening EGFR-inhibiting anti-cancer drugs. PLoS One. 2012;7(9):e42441.
37. Tomas A, Futter CE, Eden ER. EGF receptor trafficking: consequences for signaling and cancer. Trends Cell Biol. 2014;24(1):26–34.
38. Sunada H, Magun BE, Mendelsohn J, MacLeod CL. Monoclonal antibody against epidermal growth factor receptor is internalized without stimulating receptor phosphorylation. Proc Natl Acad Sci U S A. 1986;83(11):3825–29.

39. Okada Y, Kimura T, Nakagawa T, Okamoto K, Fukuya A, Goji T, Fujimoto S, Sogabe M, Miyamoto H, Muguruma N, et al. EGFR downregulation after anti-EGFR therapy predicts the antitumor effect in colorectal cancer. Mol Cancer Res. 2017;15(10):1445–54.
40. Normanno N, Maiello MR, De Luca A. Epidermal growth factor receptor tyrosine kinase inhibitors (EGFR-TKIs): simple drugs with a complex mechanism of action? J Cell Physiol. 2003;194(1):13–19.
41. Pedersen MW, Pedersen N, Ottesen LH, Poulsen HS. Differential response to gefitinib of cells expressing normal EGFR and the mutant EGFRvIII. Br J Cancer. 2005;93(8):915–23.
42. Tsien CI, Nyati MK, Ahsan A, Ramanand SG, Chepeha DB, Worden FP, Helman JI, D'Silva N, Bradford CR, Wolf GT, et al. Effect of erlotinib on epidermal growth factor receptor and downstream signaling in oral cavity squamous cell carcinoma. Head Neck. 2013;35(9):1323–30.
43. Jackman DM, Yeap BY, Sequist LV, Lindeman N, Holmes AJ, Joshi VA, Bell DW, Huberman MS, Halmos B, Rabin MS, et al. Exon 19 deletion mutations of epidermal growth factor receptor are associated with prolonged survival in non-small cell lung cancer patients treated with gefitinib or erlotinib. Clin Cancer Res. 2006;12(13):3908–14.
44. Lv C, Huang Y, Huang R, Wang Q, Zhang H, Jin J, Lu D, Zhou Y, Shen Y, Zhang W, et al. Narciclasine targets STAT3 via distinct mechanisms in tamoxifen-resistant breast cancer cells. Mol Ther Oncolytics. 2022;24:340–54.